arXiv:2108.03479v1 [hep-ph] 7 Aug 2021

LU TP 21–31
MCnet–21–13
August 2021

Forming Molecular States with Hadronic Rescattering

Philip Ilten

Department of Physics,
University of Cincinnati,
Cincinnati, OH 45221, USA

Marius Utheim

Theoretical Particle Physics,
Department of Astronomy and Theoretical Physics,
Lund University,
Sölvegatan 14A,
SE-223 62 Lund, Sweden

Abstract

A method for modelling the prompt production of molecular states using the hadronic rescattering framework of the general-purpose Pythia event generator is introduced. Production cross sections of possible exotic hadronic molecules via hadronic rescattering at the LHC are calculated for the $\chi_{c1}(3872)$ resonance, a possible tetraquark state, as well as three possible pentaquark states, $P_c^+(4312)$, $P_c^+(4440)$, and $P_c^+(4457)$. For the P_c^+ states, the expected cross section from Λ_b^0 decays is compared to the hadronic-rescattering production. The $\chi_{c1}(3872)$ cross section is compared to the fiducial $\chi_{c1}(3872)$ cross-section measurement by LHCb and found to contribute at a level of $\mathcal{O}(1\%)$. Finally, the expected yields of P_c^+ production from hadronic rescattering during Run 3 of LHCb are estimated. The prompt background is found to be significantly larger than the prompt P_c^+ signal from hadronic rescattering.

1 Introduction

While exotic bound quark states beyond the minimal $q\bar{q}$ meson and the qqq baryon structure have been proposed for some time [1–5], most experimentally observed hadrons fit these minimal bound quark configurations. Prior to the Large Hadron Collider (LHC), a number of observations for both exotic tetraquark, $qq\bar{q}\bar{q}$, and pentaquark states, $qqqq\bar{q}$, were claimed. However, many of these exotic states could not be verified by later experiments [6], excepting the Z(4430) [7] and $\chi_{c1}(3872)$ resonances [8] which remain as possible tetraquark candidates. Now with the LHC, more than 60 new hadrons have been observed with over 10 new candidates for exotic tetraquark and pentaquark states.

In 2015, the LHCb experiment discovered two resonances in the $J/\psi\,p$ mass spectrum, which were identified as possible pentaquark candidates, $P_c^+(4380)$ and $P_c^+(4450)$ [9].[1] A subsequent 2019 LHCb analysis with a larger data sample observed a possible additional resonance, $P_c^+(4312)$, and resolved the $P_c^+(4450)$ pentaquark structure as two resonances, $P_c^+(4440)$ and $P_c^+(4457)$ [10]. With this new observed mass structure, a more in-depth amplitude study of the observed $P_c^+(4380)$ resonance must be performed, leaving the existence of the $P_c^+(4380)$ state ambiguous. The three viable P_c^+ candidates, $P_c^+(4312)$, $P_c^+(4440)$, and $P_c^+(4457)$, were not observed via prompt production from the p p collision point, but rather from the decay of Λ_b^0 baryons

Similarly, the $\chi_{c1}(3872)$ state (also known as X(3872)) was first observed through B-meson decays by Belle in 2003 [8], which was later confirmed by BaBar [11]. More recently, LHCb measured the quantum numbers of the $\chi_{c1}(3872)$ to be $J^{PC} = 1^{++}$ [12,13]. Lying within 0.2 GeV of the $D^0\,\bar{D}^{*0}$ threshold, the $\chi_{c1}(3872)$ resonance is oftentimes interpreted as such a molecular state [14]. The alternative interpretation of the $\chi_{c1}(3872)$ as a four-quark state is also a possibility, but the molecular interpretation remains as the preferred model [15–21]. The $P_c^+(4312)$, $P_c^+(4440)$ and $P_c^+(4457)$ pentaquarks observed by LHCb may also be described by a molecular state of $\Sigma_c^*\,\bar{D}^0$ or $\Sigma_c^*\,\bar{D}^{*0}$ [22–30]. Other models have also been proposed for the P_c^+ states such as hadro-charmonium, a compact charmonium state bound in light hadronic matter [31].

The experimental observations above of exotic hadrons all consider production from heavy hadron decays, B-meson decays for the $\chi_{c1}(3872)$ state and Λ_b^0 for the P_c^+ states. Already, some predictions for prompt production have been made using a coalescence type model where free constituents of the molecular state may combine into a bound molecular state if close in momentum space [32, 33]. These types of models have been successful in modelling deuteron production at the LHC, including a full implementation in Pythia [34], a general-purpose event generator which allows for parameterised cross sections differential in momentum space for multiple initial states. However, these models do not consider the complete space-time picture of LHC events, and require tuning of coalescence parameters to data, whether cut-offs or overall normalisations.

Recent developments in Pythia now allow hadronic resonances to be formed from hadronic rescattering in a full space-time picture [35,36], where only the partial widths of the hadronic resonance being formed are required to fully specify the model. In this paper, this hadronic rescattering framework has been modified to predict prompt exotic hadron production for both the $\chi_{c1}(3872)$ and P_c^+ states at the LHC. The details of the models used to describe the exotic hadrons are introduced in Section 2, while results are given in Section 3 and conclusions are given in Section 4.

2 Models for exotic hadron production

The hadronic rescattering framework of Pythia can perform $2 \to 1$ scattering where the initial state hadrons combine to form a resonance hadron. The cross section of this process depends on the mass and total width of the resonance, as well as the partial width of the given channel for the resonance. In the default Pythia framework, only pre-defined resonances and rescattering channels can be used for rescattering. In this work, the framework has been expanded to allow the addition

[1] Inclusion of charge conjugate states and processes are implied throughout this work, unless explicitly noted in the text.

Table 1: Experimentally measured branching ratios for the $\chi_{c1}(3872)$, as taken from the PDG [37]. The partial widths, in MeV, for hadronic rescattering are given for each channel and are calculated as the product of the normalised branching ratio and the experimentally measured $\chi_{c1}(3872)$ width of 1.19 ± 0.21 MeV [37].

	PDG $\mathcal{B}$	width [MeV]
$D^0\,\bar{D}^{*0}$	$(3.7 \pm 0.9)\times10^{-1}$	4.3×10^{-1}
$J/\psi\,\omega$	$(4.3 \pm 2.1)\times10^{-2}$	5.0×10^{-2}
$J/\psi\,\rho^0$	$(3.8 \pm 1.2)\times10^{-2}$	4.4×10^{-2}
$\chi_{c1}\,\pi^0$	$(3.4 \pm 1.6)\times10^{-2}$	4.0×10^{-2}
$J/\psi\,\gamma$	$(8.0 \pm 4.0)\times10^{-3}$	9.3×10^{-3}
$\psi(2S)\,\gamma$	$(4.5 \pm 2.0)\times10^{-2}$	5.3×10^{-2}
$D^0\,\pi^0\,\bar{D}^0$	$(4.9\ ^{+\ 1.8}_{-\ 2.0})\times10^{-1}$	5.7×10^{-1}

of any arbitrary hadron resonance production from rescattering. Specific configurations for $\chi_{c1}(3872)$, $P_c^+(4312)$, $P_c^+(4440)$, and $P_c^+(4457)$ are then defined, given model assumptions, to determine the hadronic rescattering cross sections.

2.1 Exotic hadron properties

The $\chi_{c1}(3872)$ mass is well measured to be 3871.69 ± 0.17 MeV [37]. However, the $\chi_{c1}(3872)$ widths, both total and partial, are not as well known. In this work, the total width of the $\chi_{c1}(3872)$ is set to the world average, 1.19 ± 0.21 MeV, which is a combination of a dedicated inclusive LHCb line-shape analysis [38] and a measurement by LHCb of $\chi_{c1}(3872)$ production from B-decays [39]. The partial widths of the $\chi_{c1}(3872)$ are set by normalising the central branching ratios, $\mathcal{B}$, reported by the PDG, and multiplying these by the total width. The experimental uncertainty on these branching ratios is large, but the $D^0\,\bar{D}^{*0}$ and $D^0\,\pi^0\,\bar{D}^0$ channels dominate. Because the latter is not a two-body decay, the $\chi_{c1}(3872)$ cannot be produced in rescattering through this channel, but it still gives a significant contribution to the total cross section. Likewise, the $J/\psi\gamma$ and $\psi(2S)\gamma$ are not used for resonance formation since photons are ignored by the rescattering framework, but their contributions to the total cross section are still included. The branching ratios and partial widths used for the $\chi_{c1}(3872)$ are given in Table 1.

The masses of the P_c^+ resonances are set to the central values of the LHCb measurements. Experimental observations of the P_c^+ candidates are limited to the $p\,J/\psi$ decay channel, and so theory predictions based on a molecular model from Ref. [40] are used instead to define the total and partial widths. There, pentaquarks are treated as $\Sigma_c^+\,\bar{D}^0/\Sigma_c^+\,\bar{D}^{*0}$ molecular states, with the $P_c^+(4312)$ resonance considered as a spin-1/2 $\Sigma_c^+\,\bar{D}^0$ state. The $P_c^+(4440)$ and $P_c^+(4457)$ resonances are treated as $\Sigma_c^+\,\bar{D}^{*0}$ states, and two possible spin assignments are considered, either spin-1/2 or spin-3/2. For all spin configurations, the predicted total widths for the P_c^+ states are consistent with the observed widths, although these widths have large experimental uncertainty. Ref. [40] suggests that the $P_c^+(4440)$ resonance is most likely spin-1/2 and the $P_c^+(4457)$ resonance is spin-3/2, but notes that the opposite assignment cannot be excluded. Different form factors can also be used, and so two different models are considered in this study. Model 1 uses the (f_1, f_3) form factor set of Ref. [40], while model 2 uses the (f_2, f_3) set. Both models assume the $P_c^+(4440)$ resonance is spin-1/2 and the $P_c^+(4457)$ resonance is spin-3/2. The pentaquark partial widths used in this paper are summarised in Table 2.

2.2 Exotic hadron production from rescattering

In the hadronic rescattering framework of Pythia, two hadrons will interact if they pass each other in their centre-of-mass (CM) frame with an impact parameter $b < \sqrt{\sigma/\pi}$, where σ is the total cross section depending on the particle species and the CM energy. When two particles do interact, the

Table 2: Partial widths in MeV for each pentaquark state of the two models considered from Ref. [40]. For both models the $P_c^+(4440)$ is chosen to be spin-1/2 while the $P_c^+(4457)$ is chosen to be spin-3/2.

	model 1 width [MeV]			model 2 width [MeV]		
	$P_c^+(4312)$	$P_c^+(4440)$	$P_c^+(4457)$	$P_c^+(4312)$	$P_c^+(4440)$	$P_c^+(4457)$
$\Lambda_c^+ \bar{D}^0$	6.0×10^{-2}	5.6	1.5	3.0×10^{-1}	2.7	1.2
$\Lambda_c^+ \bar{D}^{*0}$	3.8	1.4×10^{1}	6.1	1.1×10^{1}	1.2×10^{1}	6.9
$\Sigma_c^+ \bar{D}^0$	–	3.4	1.0	–	3.4	9.0×10^{-1}
$\Sigma_c^{*+} \bar{D}^0$	–	8.0×10^{-1}	6.2	–	9.0×10^{-1}	7.2
$n\,\pi^+$	2.0×10^{-3}	1.0×10^{-3}	5.0×10^{-5}	8.5×10^{-1}	1.0×10^{-1}	3.0×10^{-1}
$n\,\rho^+$	2.0×10^{-5}	1.5×10^{-4}	1.0×10^{-5}	4.0×10^{-4}	2.0×10^{-1}	5.0×10^{-2}
$p\,\pi^0$	2.0×10^{-3}	1.0×10^{-3}	5.0×10^{-5}	8.5×10^{-1}	1.0×10^{-1}	3.0×10^{-1}
$p\,\rho^0$	2.0×10^{-5}	1.5×10^{-4}	1.0×10^{-5}	4.0×10^{-4}	2.0×10^{-1}	5.0×10^{-2}
$p\,\omega$	1.0×10^{-4}	1.0×10^{-4}	9.0×10^{-5}	3.0×10^{-3}	1.5	4.0×10^{-1}
$p\,\eta_c$	1.0×10^{-2}	3.0×10^{-4}	6.0×10^{-5}	4.0×10^{-1}	7.0×10^{-2}	3.0×10^{-3}
$p\,J/\psi$	1.0×10^{-3}	3.0×10^{-2}	1.0×10^{-2}	1.0×10^{-1}	6.0×10^{-1}	6.0×10^{-1}
$p\,\chi_{c0}$	–	8.0×10^{-4}	3.0×10^{-5}	–	1.0×10^{-1}	3.0×10^{-3}

specific process to simulate is chosen with a probability proportional to the partial cross section of that process. Since rescattering in Pythia increases the charged particle multiplicity, the recommendation of Ref. [35] is followed, where setting $p_{\perp 0}$ parameter of the multi-parton interaction (MPI) framework to 2.345 GeV compensates for this effect. This reduces the event multiplicity before rescattering, with respect to the default Pythia MPI tune.

For processes involving charm hadrons, the total cross section in Pythia is calculated using the additive quark model (AQM) [41, 42]. In this model, the total cross section for two initial hadrons A and B is given by

$$\sigma_{\mathrm{AQM,tot}} = (40\ \mathrm{mb})\frac{n_{\mathrm{eff},A}}{3}\frac{n_{\mathrm{eff},B}}{3}, \tag{1}$$

where n_{eff} is the effective number of quarks in each hadron. In Pythia, this number is defined from the quark numbers of the hadron, and by default is

$$n_{\mathrm{eff}} = n_{\mathrm{u}} + n_{\mathrm{d}} + 0.6n_{\mathrm{s}} + 0.2n_{\mathrm{c}} + 0.07n_{\mathrm{b}}. \tag{2}$$

As an example, the total $p\,J/\psi$ cross section determined by the AQM is $\sigma_{\mathrm{AQM,tot}} = 5.33$ mb. The cross section for elastic scattering (in mb) is also determined with AQM,

$$\sigma_{\mathrm{AQM,el}} = 0.039\sigma_{\mathrm{AQM}}^{3/2}. \tag{3}$$

The difference between the total AQM cross section and the elastic AQM cross section gives an inelastic AQM cross section of

$$\sigma_{\mathrm{AQM,inel}} = \sigma_{\mathrm{AQM,tot}} - \sigma_{\mathrm{AQM,el}}, \tag{4}$$

which in default Pythia corresponds to diffractive and non-diffractive interactions.

In the model of Ref. [40], pentaquarks can in principle also form in $n\,\rho^0$, $p\,\rho^0$, or $p\,\omega$ interactions. Pythia also uses the AQM model for the total cross section of these processes, but pentaquark formation through these processes is so rare that the contribution will be negligible. Finally, pentaquarks can be produced in nucleon–pion interactions, *i.e.* the $n\,\pi^+$ and $p\,\pi^0$ channels. The formation probability is also very small here, but now the contribution may be non-negligible due to the abundance of these particles in LHC collisions. For these processes, the total cross sections at energies near the pentaquark masses are given by the $\mathrm{HPR_1R_2}$ parameterisation [43].

The partial cross section for a resonance formation process $AB \to R$ is given by a nonrelativistic Breit–Wigner [43],

$$\sigma_{\mathrm{res}} = \frac{\pi}{p_{\mathrm{CM}}^2}\frac{(2S_R+1)}{(2S_A+1)(2S_B+1)}\frac{\Gamma_{R\to AB}\Gamma_R}{(m_R - E_{\mathrm{CM}})^2 + \frac{1}{4}\Gamma_R^2}, \tag{5}$$

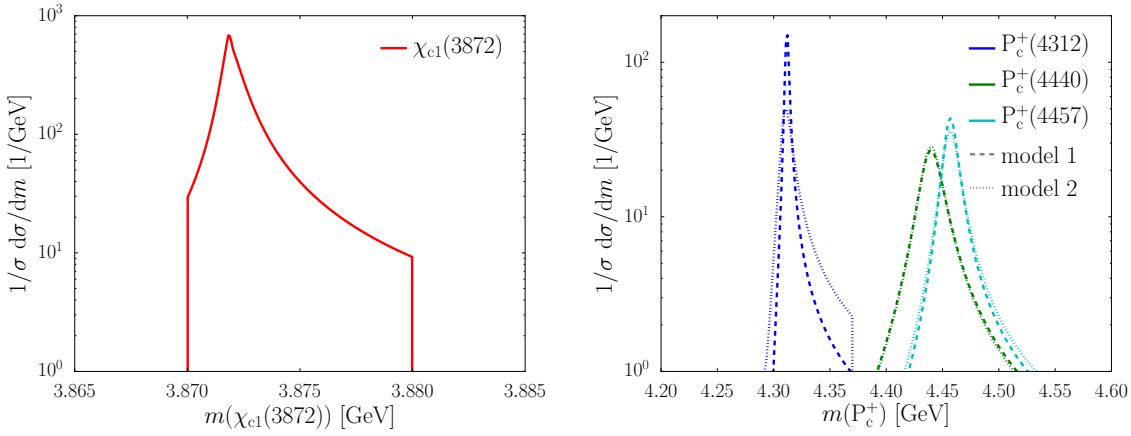

Figure 1: Mass distributions for the (left) $\chi_{c1}(3872)$ tetraquark and (right) P_c^+ pentaquarks.

where p_{CM} and E_{CM} are the momentum and energy of the incoming particles in their CM frame, S is the spin of each particle, and m_R and Γ_R, $\Gamma_{R\to AB}$ are the mass, total width, and partial width of the resonance, respectively. These widths are mass dependent, as described in Ref. [44], giving mass distributions as shown in Figure 1. Using these widths can give mass distributions with longer tails than are physically reasonable, and therefore explicit mass bounds are required. These explicit cut-offs can give discontinuities in the mass distribution, but this is not expected to significantly affect any relevant physical observables.

It is important to keep in mind that resonance formation does not change the mass spectrum when the decay products are the same as the incoming particles. For instance, the process $\Lambda_c^+\bar{\mathrm{D}} \to \mathrm{P}_c^+(4440) \to \Lambda_c^+\bar{\mathrm{D}}$ will not change the $\Lambda_c^+\bar{\mathrm{D}}$ mass spectrum, as they must already be correlated in order to form the resonance. However, in a system out of equilibrium, resonances can change the relative composition of particles. If resonance production receives a significant contribution from a particular channel, *e.g.* $\mathrm{p}\,\pi^0$ where the flux is large, but their decays are dominated by a different channel, *e.g.* $\mathrm{P}_c^+ \to \Lambda_c^+\bar{\mathrm{D}}$, then a peak structure would be appear in that decay channel.

When resonance formation is possible, the total cross section is fixed, and $\sigma_{\mathrm{AQM,inel}}$ is reduced by the resonance cross section. If σ_{res} is greater than $\sigma_{\mathrm{AQM,inel}}$, the total cross section is increased to $\sigma_{\mathrm{res}} + \sigma_{\mathrm{AQM,el}}$, which as an example, occurs for the $\Lambda_c^+\bar{\mathrm{D}}^{*0} \to \mathrm{P}_c^+(4312)$ process. The cross sections for tetraquark and pentaquark resonances, as a function of the rescattering centre-of-mass energy, are shown in Figure 2 for the primary rescattering channels. Some of these cross sections grow very large near the kinematic threshold of the channel, which is particularly visible for $\mathrm{D}^0\,\bar{\mathrm{D}}^{*0} \to \chi_{c1}(3872)$. The technical reason for this is that the lower mass bound for the particle lies below the threshold so the width does not vanish, hence the factor $1/p_{\mathrm{CM}}^2$ in Equation 5 dominates. Physically, this can be motivated by the fact that slow-moving particles spend more time near each other, and have a larger chance of interacting. For the $\chi_{c1}(3872)$ resonance, however, the cross section grows larger than what might be considered reasonable considering the range of strong interactions. In the rescattering framework, the range of interactions is capped at a generous 5 fm, corresponding to a cross section of roughly 785 mb, which limits the $\chi_{c1}(3872)$ cross section. The interpretation of such extremely large cross sections is not clear, but a more detailed handling is outside the scope of this study.

2.3 Pentaquark production from Λ_b^0 decays

While the focus of this study is exotic hadron production from hadronic rescattering, it is useful in the context of the P_c^+ states to compare these prompt production cross sections with the expected cross sections from Λ_b^0 decays. The branching ratios of the Λ_b^0 into P_c^+ states have not been experimentally

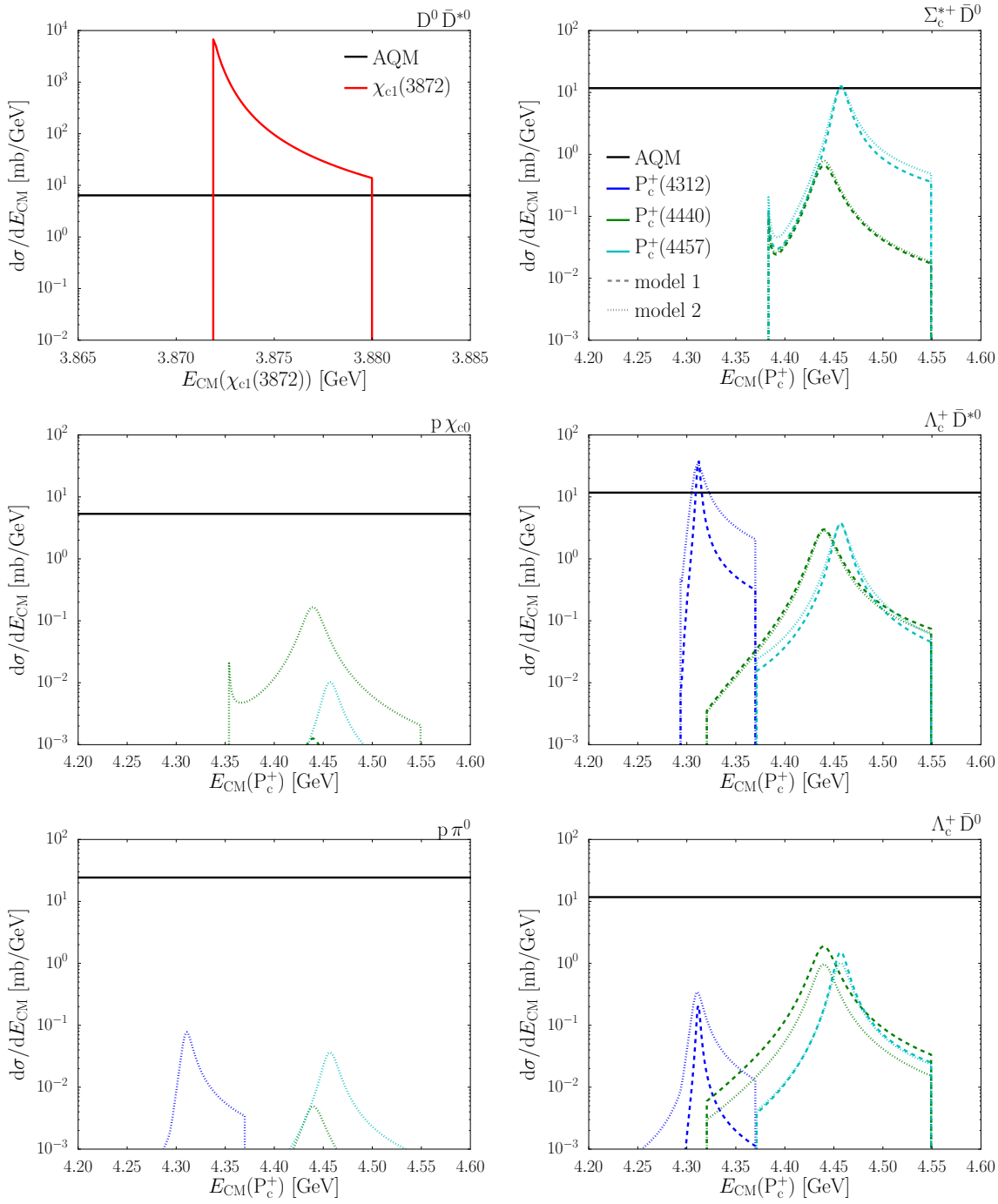

Figure 2: Cross sections of the tetraquark and pentaquark resonance formation for relevant two-particle rescattering channels. The (solid black) total AQM cross section corresponds to the Pythia default in the absence of exotic hadrons, and while drawn across the entire E_{CM} range is only available above mass threshold for each resonance. For the pentaquarks, cross sections are calculated using (dashed) model 1 and (dotted) model 2 given Table 2.

Table 3: Branching ratios for $\Lambda_b^0 \to P_c^+ K^-$, determined using $\mathcal{R}$ [10] and $\mathcal{B}(\Lambda_b^0 \to p J/\psi K^-)$ [45] from data, and $\mathcal{B}(P_c^+ \to p J/\psi)$ calculated from Table 2. Both $\mathcal{R}$ and $\mathcal{B}(P_c^+ \to p J/\psi)$ are listed for each pentaquark state, where the individual uncertainties on $\mathcal{R}$ have been combined in quadrature.

	$P_c^+(4312)$	$P_c^+(4440)$	$P_c^+(4457)$
$\mathcal{R}$	$(3.0\ ^{+\ 3.5}_{-\ 1.1})\times10^{-3}$	$(1.1\ ^{+\ 0.4}_{-\ 0.3})\times10^{-2}$	$(5.3\ ^{+\ 2.2}_{-\ 2.1})\times10^{-3}$
model 1 $\mathcal{B}(\Lambda_b^0 \to P_c^+ K^-)$	3.7×10^{-3}	2.8×10^{-3}	2.5×10^{-3}
$\mathcal{B}(P_c^+ \to p J/\psi)$	2.6×10^{-4}	1.3×10^{-3}	6.8×10^{-4}
model 2 $\mathcal{B}(\Lambda_b^0 \to P_c^+ K^-)$	1.3×10^{-4}	1.3×10^{-4}	5.1×10^{-5}
$\mathcal{B}(P_c^+ \to p J/\psi)$	7.6×10^{-3}	2.7×10^{-2}	3.4×10^{-2}

measured, but can be fully determined given the partial widths of Table 2 and the results of Ref. [10]. Here the contribution ratio is defined as

$$\mathcal{R} = \frac{\mathcal{B}(\Lambda_b^0 \to P_c^+ K^-)\,\mathcal{B}(P_c^+ \to p J/\psi)}{\mathcal{B}(\Lambda_b^0 \to p J/\psi K^-)}, \tag{6}$$

and has been measured for each P_c^+ resonance. The branching ratio in the denominator is set as the experimentally measured value of $\mathcal{B}(\Lambda_b^0 \to p J/\psi K^-) = (3.2^{+0.6}_{-0.5}) \times 10^{-4}$ [45]. By considering $\mathcal{B}(P_c^+ \to p J/\psi)$ for each pentaquark state as set by Table 2, the relevant Λ_b^0 branching ratios can be determined by

$$\mathcal{B}(\Lambda_b^0 \to P_c^+ K^-) = \mathcal{B}(\Lambda_b^0 \to p J/\psi K^-)\frac{\mathcal{R}}{\mathcal{B}(P_c^+ \to p J/\psi)}. \tag{7}$$

Values of $\mathcal{R}$ for each pentaquark state are also taken from experiment [10] and are given in Table 3, where the Λ_b^0 branching ratios are also provided. Note that in model 1, the branching ratios for $P_c^+ \to p J/\psi$ are lower than for model 2 by an order of magnitude or more, which gives a much smaller $\Lambda_b^0 \to P_c^+ K^-$ branching ratio for the former.

3 Results

The cross sections of Figure 2 are not production cross sections, but instead must be combined with the relevant flux of initial state particles which can rescatter to produce molecular states. High multiplicity environments are necessary to provide a sufficiently large initial state flux, and so high energy hadronic collisions, such as those produced at the LHC, are an ideal laboratory to study possible molecular state formation from hadronic rescattering. During Run 1, the LHC collided proton-proton beams at $\sqrt{s} = 7$ and 8 TeV, while during Run 2 $\sqrt{s} = 13$ TeV, which corresponds to the majority of the LHC data set. During Run 3, the LHC is expected to run at a CM energy of 14 TeV, although 13 TeV may also be used, depending upon the performance of the collider. Consequently, a configuration with $\sqrt{s} = 13$ TeV p p collisions is conservatively chosen for this study, since particle flux also increases as $\sqrt{s}$ is increased.

Using the default Pythia parameter tune [46] and a modified version of Pythia 8.306, the average visible final state particle multiplicity for inelastic LHC events at $\sqrt{s} = 13$ TeV is expected to be $\mathcal{O}(200)$, with an inelastic cross-section of 78 mb. This predicted inelastic cross-section is in good agreement with LHC measurements [47, 48], including forward measurements from LHCb [49] and TOTEM [50]. The predicted particle density and energy flow distributions also describe experimental LHC data well [51–54], across a number of experimental event categorisations intended to separate elastic, diffractive, and inelastic scattering. Individual particle species are also typically described well [55, 56], including open-charm meson production [57], although experimental measurements for many rare mesons and baryons are not available for direct comparison.

The light pseudo-scalar mesons, π^0 and $\pi^\pm$, each have an average multiplicity of $\mathcal{O}(50)$, while the average multiplicity for light meson and baryons is at the level of $\mathcal{O}(10)$ per species. This includes the ρ^0, $\rho^\pm$, and ω vector mesons, and the $\mathrm{p}/\bar{\mathrm{p}}$ and $\mathrm{n}/\bar{\mathrm{n}}$ light baryons. The $\mathrm{D}^0/\bar{\mathrm{D}}^0$ and $\mathrm{D}^{*0}/\bar{\mathrm{D}}^{*0}$ mesons each contribute at an average multiplicity of $\mathcal{O}(10^{-1})$, while the $\Lambda_\mathrm{c}^\pm$ contributes at an average multiplicity of $\mathcal{O}(10^{-2})$. The relevant quarkonia states, J/ψ and $\chi_{\mathrm{c}0}$, have average multiplicities of $\mathcal{O}(10^{-3})$, where both colour octet and singlet contributions are included. For the J/ψ meson, feed-down production from both χ_c-meson and B-hadron decays is also included. The η_c contribution is significantly less at $\mathcal{O}(10^{-4})$, but this is a known underestimation by Pythia, since production is included only through hadronization and not through direct nonrelativistic QCD (NRQCD) calculations.

The production of both $\Sigma_\mathrm{c}^\pm$ and $\Sigma_\mathrm{c}^{*\pm}$ baryons is relatively rare, with average multiplicities of $\mathcal{O}(10^{-4})$ and $\mathcal{O}(10^{-3})$, respectively. The production of $\Lambda_\mathrm{b}^0/\bar{\Lambda}_\mathrm{b}^0$, relevant for displaced production of pentaquark states, is also rare with an average multiplicity of $\mathcal{O}(10^{-3})$. Given these average multiplicities, the $\mathrm{D}^0\,\bar{\mathrm{D}}^{*0}$ rescattering channel is expected to dominate $\chi_{\mathrm{c}1}(3872)$ production, while the rescattering channels with Λ_c^+ baryons are expected to dominate P_c^+ production. If the rescattering probability for the Λ_c^+ channels, which depends on the kinematics of the scattering hadrons, is similar to the $\Lambda_\mathrm{b}^0 \to \mathrm{P}_\mathrm{c}^+\,\mathrm{K}^-$ branching ratio, then P_c^+ production via hadronic rescattering and Λ_b^0 decays is expected to have roughly similar rates.

3.1 Differential cross-sections

The cross sections for tetraquark and pentaquark production at the LHC with $\sqrt{s} = 13$ TeV are provided differentially in $p_\perp$ and rapidity by Figure 3 and Figure 4, respectively. The cross sections are separated by rescattering channel, where the first four channels of Figure 2 are shown. For the $\chi_{\mathrm{c}1}(3872)$, only the dominant $\mathrm{D}^0\,\bar{\mathrm{D}}^{*0}$ channel is given although both $\mathrm{J}/\psi\,\omega$ and $\mathrm{J}/\psi\,\rho^0$ channels do contribute, but at $\mathcal{O}(10^{-2})$ the rate of $\mathrm{D}^0\,\bar{\mathrm{D}}^{*0}$ production. For the $\mathrm{P}_\mathrm{c}^+(4312)$ and $\mathrm{P}_\mathrm{c}^+(4440)$ resonances the $\Lambda_\mathrm{c}^+\,\bar{\mathrm{D}}^{*0}$ channel is the leading production mechanism, while the $\Sigma_\mathrm{c}^*\,\bar{\mathrm{D}}^0$ channel is the dominant channel for $\mathrm{P}_\mathrm{c}^+(4457)$ production. The $\Sigma_\mathrm{c}^+\,\bar{\mathrm{D}}^0$ channel contributes to $\mathrm{P}_\mathrm{c}^+(4440)$ and $\mathrm{P}_\mathrm{c}^+(4457)$ production for both models, but is always subleading. The channels with light baryons do not significantly contribute to pentaquark production except the $\mathrm{p}\,\chi_{\mathrm{c}0}$ channel for the model 2 $\mathrm{P}_\mathrm{c}^+(4440)$ state. Note that the $\mathrm{p}\,\mathrm{J}/\psi$ discovery channel is not relevant for P_c^+ production.

The $p_\perp$ distributions of both the $\chi_{\mathrm{c}1}(3872)$ and P_c^+ states peak near 2 GeV. However, the $\mathrm{p}\,\chi_{\mathrm{c}0}$ channel is significantly softer than the other channels, peaking near 1 GeV. It is important to note that the production of the $\chi_{\mathrm{c}0}$ in Pythia is via a hard NRQCD matrix element, *e.g.* $\mathrm{g}\,\mathrm{g} \to \mathrm{g}\,\chi_{\mathrm{c}0}$, where the low $p_\perp$ divergence has been regulated with a $p_\perp$ damping term. This is in contrast to the other hadrons, which are produced directly from the hadronization process. The rapidity distribution for the $\chi_{\mathrm{c}1}(3872)$ peaks centrally as do the P_c^+ rapidity distributions, although the P_c^+ distributions are slightly broader.

The total hadronic-rescattering cross sections for the pentaquarks are compared to the expected cross section from Λ_b^0 decays in Figure 5. In general, the $p_\perp$ distributions between hadronic rescattering and Λ_b^0 decays are similar, and again tend to peak around 2 GeV. For the model 2 $\mathrm{P}_\mathrm{c}^+(4440)$ state, the $\mathrm{p}\,\chi_{\mathrm{c}0}$ channel contributes at the same level as the $\Lambda_\mathrm{c}^+\,\bar{\mathrm{D}}^{*0}$ channel. This results in the softer $\mathrm{P}_\mathrm{c}^+(4440)$ $p_\perp$ spectrum of model 2 in comparison to model 1. The rapidity distributions for P_c^+ states produced from Λ_b^0 decays are more central than for those produced in rescattering. For the former, this primarily depends upon the rapidity of the parent Λ_b^0 baryons, which in turn depend upon the jets from which they are produced. For the latter, the distributions are broader, and there is a rapidity dip around zero for the $\mathrm{P}_\mathrm{c}^+(4457)$ state.

This dip is particularly pronounced in channels with lighter hadrons, *e.g.* $\mathrm{p}\,\pi^0$, whose total contribution to pentaquark formation is very small overall. Similar dips also appear in the rapidity spectrum of $\mathrm{p}\,\pi^0$ rescatterings with invariant masses around the pentaquark masses, regardless of whether pentaquarks are actually formed. Hence, this is a general feature of the rescattering framework, and not specific to pentaquarks. Light hadrons must have a more pronounced difference in momenta in order to reach the invariant masses necessary for pentaquark formation. Consequently, the rapidity difference

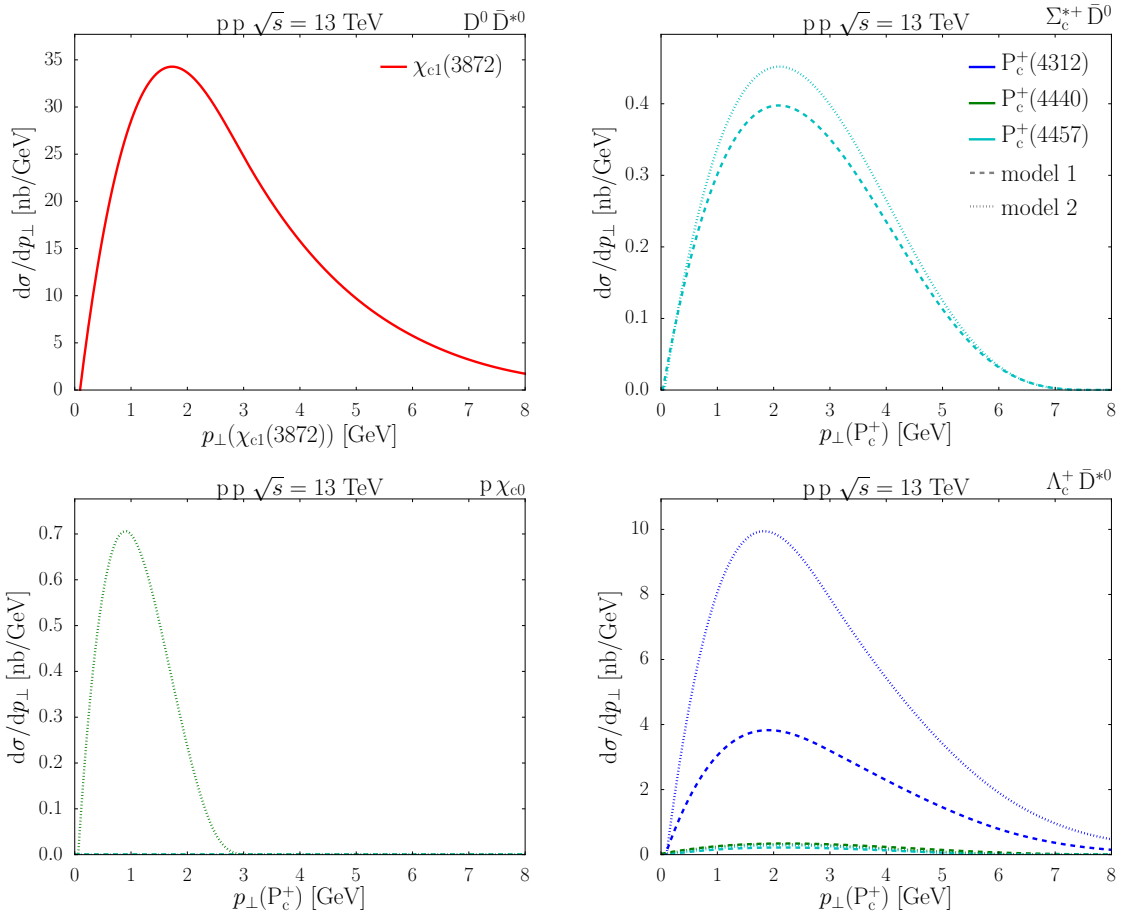

Figure 3: Tetraquark and pentaquark resonance hadronic-rescattering cross sections, differential in resonance $p_\perp$, produced in p p collisions at $\sqrt{s} = 13$ TeV.

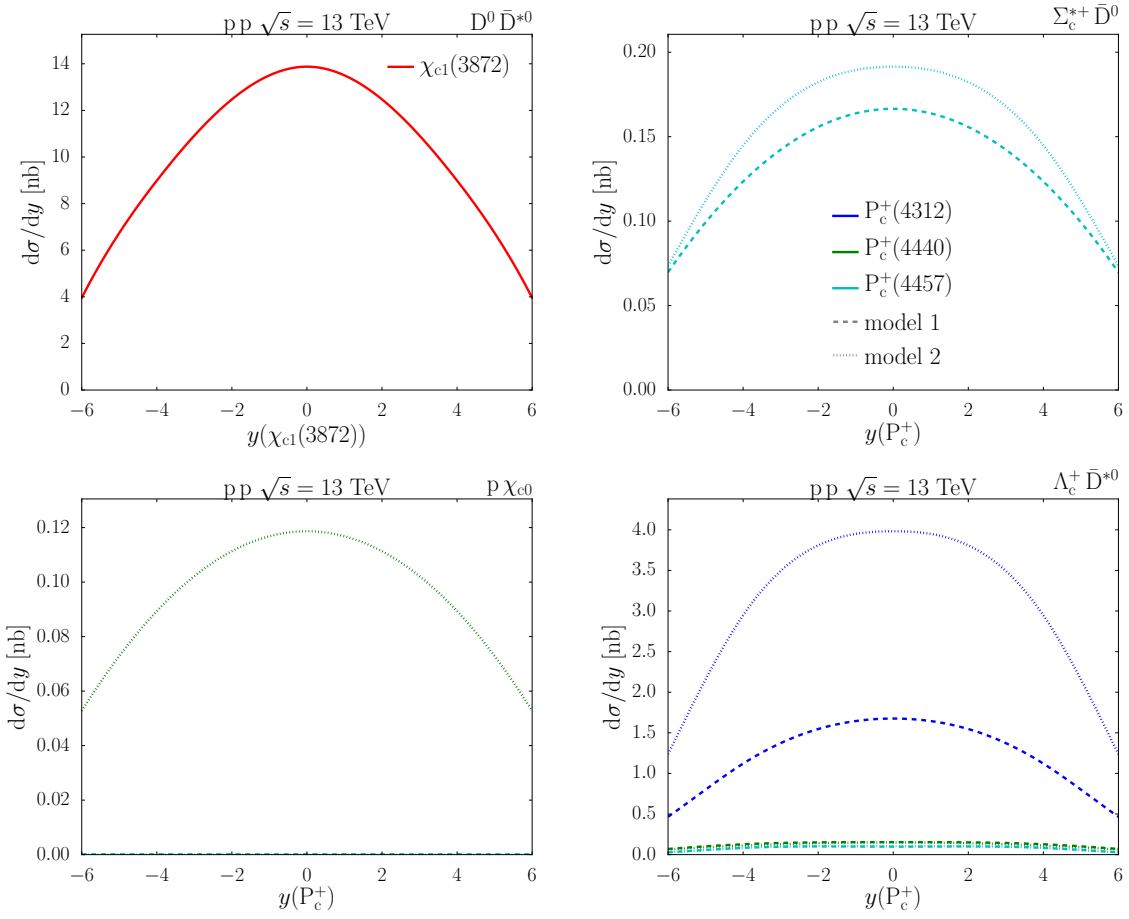

Figure 4: Tetraquark and pentaquark resonance hadronic-rescattering cross sections, differential in resonance y, produced in p p collisions at $\sqrt{s} = 13$ TeV.

between the rescattering particles should be non-zero, although this still does not fully explain why the total momentum also has non-zero rapidity. Since this is a matter of rescattering in general, and has only a small effect on exotic hadrons, a more in-depth study is left for the future.

The cross sections for $\mathrm{P_c^+}$ from rescattering are generally similar between the two models, which is expected since the dominant partial widths remain similar between the models. The cross section from Λ_b^0 decays differs significantly between the two models, however. This is because the J/ψ partial widths, used in determining $\mathcal{B}(\Lambda_\mathrm{b}^0 \to \mathrm{P_c^+\,K^-})$, differ by $\mathcal{O}(10)$ to $\mathcal{O}(100)$. This has important experimental implications. Measuring the Λ_b^0 cross section in conjunction with the $\Lambda_\mathrm{b}^0 \to \mathrm{P_c^+\,K^-}$ production can help separate molecular state models, with expected differences as large as $\mathcal{O}(100)$.

3.2 Tetraquarks with LHCb

The fiducial cross section for $\chi_{\mathrm{c1}}(3872)$ production in $\mathrm{p\,p}$ collisions at a centre-of-mass energy of $\sqrt{s} = 7$ TeV has been measured by LHCb [58] to be,

$$\sigma_{\mathrm{LHCb}}(\mathrm{p\,p} \to \chi_{\mathrm{c1}}(3872)[\to \mathrm{J}/\psi\,\pi^+\,\pi^-] + X) = 5.4 \pm 1.3 \pm 0.8 \text{ nb}$$

where the $\chi_{\mathrm{c1}}(3872) \to \mathrm{J}/\psi\,\rho^0$ final state with a $\rho^0 \to \pi^+\,\pi^-$ decay has been used. For this fiducial cross section, the pseudorapidity of the $\chi_{\mathrm{c1}}(3872)$ is required to be in the range $2.0 \leq \eta \leq 4.5$, and its momentum must be in the range $5 \leq p_\perp \leq 20$ GeV. These requirements ensure efficient detection of the final state and help minimise systematic uncertainties due to particle reconstruction inefficiencies. This cross section does not separate the prompt $\chi_{\mathrm{c1}}(3872)$ production from feed-down production, where the $\chi_{\mathrm{c1}}(3872)$ is produced from the decay of a heavier hadron. Indeed, $\chi_{\mathrm{c1}}(3872)$ production from B-hadron decays is expected to be sizeable.

The predicted cross section for $\chi_{\mathrm{c1}}(3872)$ production from hadronic rescattering in $\mathrm{p\,p}$ collisions at $\sqrt{s} = 7$ TeV is,

$$\sigma_{\mathrm{rescatter}}(\mathrm{p\,p} \to \chi_{\mathrm{c1}}(3872)[\to \mathrm{J}/\psi\,\pi^+\,\pi^-] + X) = 0.04 \text{ nb}$$

where the uncertainty on this cross section will have contributions from the uncertainty of the $\mathrm{D^0}/\bar{\mathrm{D}}^0$ and $\mathrm{D^{*0}}/\bar{\mathrm{D}}^{*0}$ meson fluxes, and the uncertainty of the estimated hadronic rescattering cross sections. The former uncertainty depends upon the tuning of Pythia used, while the latter depends not only on the modelling of the $\chi_{\mathrm{c1}}(3872)$ line-shape but also the partial widths for each rescattering channel. Both of these uncertainties are difficult to quantify and so the hadronic rescattering cross section is quoted here without uncertainty, with the explicit understanding that the uncertainty may be large.

The predicted hadronic-rescattering cross section is not larger than the measured total cross section, which lends some credence to this hadronic-rescattering model. However, the hadronic-rescattering cross section is $\mathcal{O}(100)$ times less than the measured cross section, indicating that hadronic rescattering is expected to provide a negligible contribution to $\chi_{\mathrm{c1}}(3872)$ production. Utilising lifetime measurement capabilities, future LHCb measurements could separate the $\chi_{\mathrm{c1}}(3872)$ cross-section into prompt and feed-down production, allowing for a direct comparison with this prediction. This could help determine how best to model prompt $\chi_{\mathrm{c1}}(3872)$ formation, whether from direct NRQCD calculations, parton showers, hadronization, hadronic rescattering, *etc.*

3.3 Pentaquarks with LHCb

While pentaquark production has been unambiguously observed by LHCb using the exclusive $\Lambda_\mathrm{b}^0 \to \mathrm{p\,J}/\psi\,\mathrm{K^-}$ decay, no $\mathrm{P_c^+}$ cross sections from Λ_b^0 decays or otherwise, have been measured. To fully understand the nature of the observed pentaquark states, these measurements are necessary, including separate cross-section measurements of prompt and feed-down pentaquark production. Depending upon the expected rate of prompt pentaquark production, this may be challenging, as there can be large combinatorial backgrounds when considering a prompt pentaquark signal. The displaced vertex, $\mathrm{K^-}$ in the final state, and Λ_b^0 mass constraint are all no longer available when searching for prompt

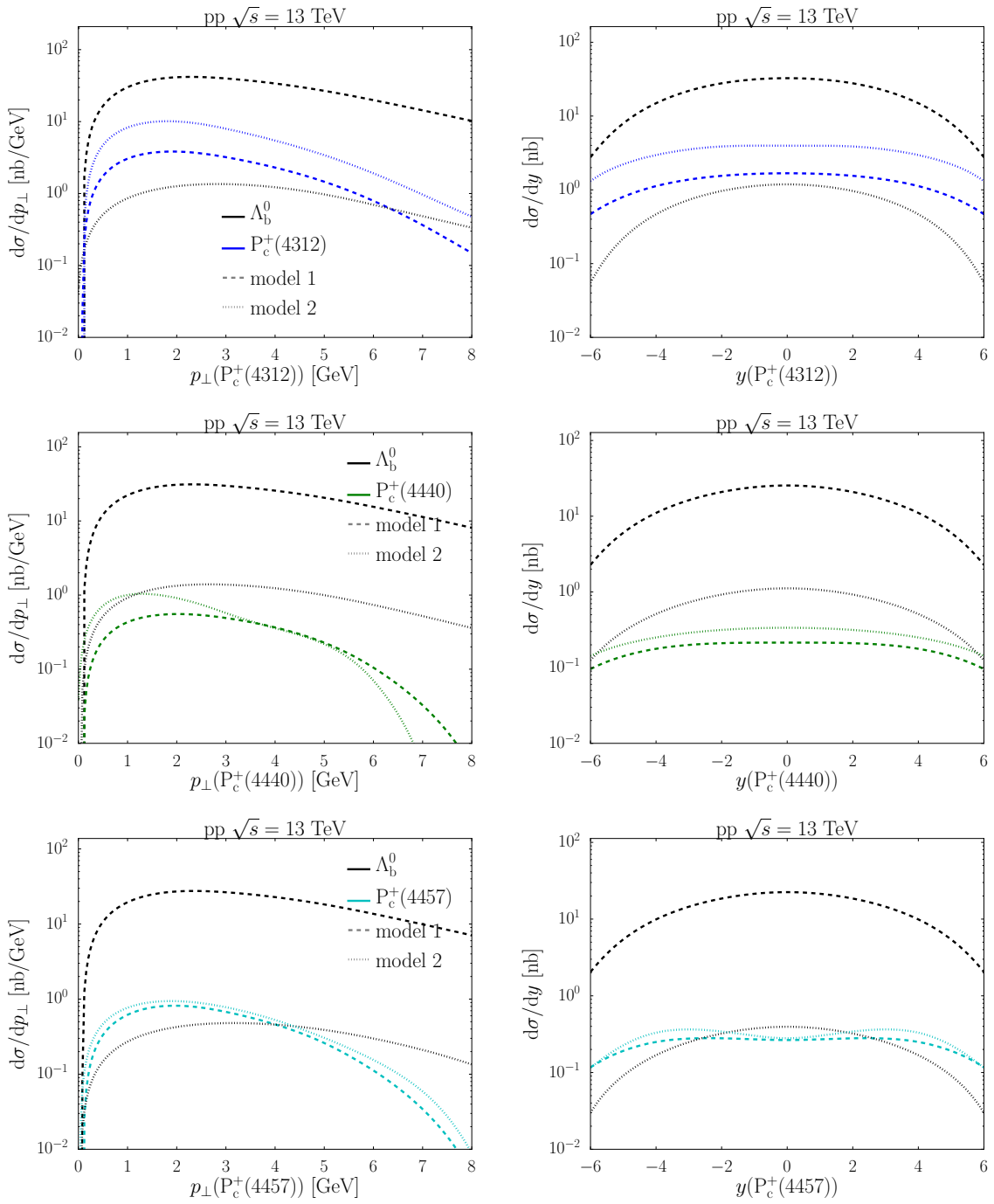

Figure 5: Total hadronic-rescattering cross-section for (dashed) model 1 and (dotted) model 2 pentaquarks, compared to pentaquark production from (black) Λ_b^0 decays.

pentaquark candidates. Consequently, a clean and fully reconstructed final state of charged particles is preferred to reduce these backgrounds.

For the model 1 $\mathrm{P_c^+}(4312)$, the largest branching fraction for an exclusive charged final state is $\mathcal{O}(10^{-4})$ with at least five charged particles, including two or more $\pi^{\pm}$. The combinatorial backgrounds for such a final state will be large, and the high multiplicity will also result in relatively low momentum charged particles that are difficult to reconstruct. The $\mathrm{p}\,\eta_\mathrm{c}[\to \mathrm{K^+}\,\mathrm{K^-}]$ final state is expected to have a branching ratio of $\mathcal{O}(10^{-5})$, while the $\mathrm{p}\,\mathrm{J}/\psi[\to \mu^+\,\mu^-]$ branching ratio will be $\mathcal{O}(10^{-6})$. For the model 1 $\mathrm{P_c^+}(4440)$, the branching ratio for the $\mathrm{p}\,\mathrm{J}/\psi[\to \mu^+\,\mu^-]$ final state is $\mathcal{O}(10^{-4})$, where all fully charged final states with higher branching ratios up to $\mathcal{O}(10^{-3})$ have multiplicities of five or larger. The situation for the $\mathrm{P_c^+}(4457)$ is similar, but with the relevant branching ratios reduced by an order of magnitude. Consequently, without detailed background and detector simulation, the $\mathrm{P_c^+} \to \mathrm{p}\,\mathrm{J}/\psi[\to \mu^+\,\mu^-]$ decay still provides a reasonable final state for the model 1 pentaquarks.

The discovery channel of $\mathrm{p}\,\mathrm{J}/\psi$ is enhanced in model 2 by $\mathcal{O}(10)$ to $\mathcal{O}(100)$ with respect to model 1. For all model 2 pentaquarks, the $\mathrm{p}\,\mathrm{J}/\psi[\to \mu^+\,\mu^-]$ final state branching ratios are the same order of magnitude as the leading branching ratios, which for the $\mathrm{P_c^+}(4440)$ and $\mathrm{P_c^+}(4457)$ are in the $\mathrm{p}\,\rho^0[\to \pi^+\,\pi^-]$ channel. The $\mathrm{p}\,\mathrm{J}/\psi[\to \mu^+\,\mu^-]$ branching ratio is $\mathcal{O}(10^{-4})$ for the $\mathrm{P_c^+}(4312)$ and $\mathcal{O}(10^{-3})$ for the $\mathrm{P_c^+}(4440)$ and $\mathrm{P_c^+}(4457)$ states. The $\mathrm{p}\,\mathrm{J}/\psi[\to \mathrm{e^+}\,\mathrm{e^-}]$ branching ratios are also the same as the $\mathrm{p}\,\mathrm{J}/\psi[\to \mu^+\,\mu^-]$ branching ratios, but in the context of LHCb, electron reconstruction and identification is significantly more challenging than for muons.

This study considers using the LHCb detector to measure prompt pentaquark production via hadronic rescattering. The Run 3 LHCb detector [59–64] is a forward arm spectrometer with full particle reconstruction between pseudorapidities of 2 and 5, including a precision vertex detector, a charged particle tracking system, Cherenkov detectors providing particle identification, an electromagnetic calorimeter, and a muon system. Additionally, during Run 3 the LHCb data acquisition system will employ a real-time analysis strategy [63], where the entire detector will be read out and calibrated in real time. This will enable the full reconstruction of pentaquark candidates during online data taking, and minimise possible inefficiencies of data acquisition. The target Run 3 integrated luminosity for LHCb of 15 fb^{-1} at $\sqrt{s} = 13$ TeV is assumed for this study [64].

Selecting the $\mathrm{p}\,\mathrm{J}/\psi[\to \mu^+\,\mu^-]$ final state, the following LHCb fiducial requirements are made: the muons and protons must have $2 < \eta < 5$; the muons must have $p_\perp > 0.5$ GeV; and the proton must have $p_\perp > 1$ GeV. Given this fiducial selection, and assuming similar performance to the Run 2 detector [65], the reconstruction efficiency is expected to be near 100%. The background is evaluated as combinations of prompt real $\mathrm{J}/\psi[\to \mu^+\,\mu^-]$ decays with prompt protons. Background from particle mis-identification will also contribute, but is expected to be subleading. Real displaced $\mathrm{P_c^+}$ signals can be separated from the prompt $\mathrm{P_c^+}$ signal with fits to lifetime observables.

Comparisons of the background distributions with the signal distributions are shown in Figure 6 with only the final state pseudorapidity requirements in place. All $p_\perp$ distributions are similar between the $\mathrm{P_c^+}$ states, except for the model 2 $\mathrm{P_c^+}(4440)$ state, due to the contribution of the $\mathrm{p}\,\chi_{\mathrm{c0}}$ channel. The muon $p_\perp$ is slightly softer for the signal than for the background, while the proton $p_\perp$ is slightly harder for the signal than the background. However, these differences are not sufficiently pronounced to provide any kinematic discrimination. Further separation of signal and background may be possible, but would require detailed detector simulation more suitable within an experimental context. The $\mathrm{P_c^+}$ candidate mass distribution peaks near the nominal $\mathrm{P_c^+}$ masses, which complicates resonance fitting. Increasing the $p_\perp$ requirement on the proton could flatten this distribution, but will reduce the signal selection efficiency.

The LHCb $\mu^+\,\mu^-$ mass resolution is roughly 0.4% of the dimuon mass [65]. Even assuming twice the resolution for the three-body $\mathrm{P_c^+}$ candidate with the inclusion of the proton, this is well below the natural width of the $\mathrm{P_c^+}$ states. Consequently, a mass window of roughly six times the $\mathrm{P_c^+}$ total width is used when determining the number of expected background candidates. The expected number of signal and background candidates is given in Table 4. The mass window of $4.4 < m < 4.5$ GeV is considered for the background when comparing to all three $\mathrm{P_c^+}$ states. The number of background candidates will vary slightly given different $\mathrm{P_c^+}$ pole masses, but for the purposes of this study this approximation

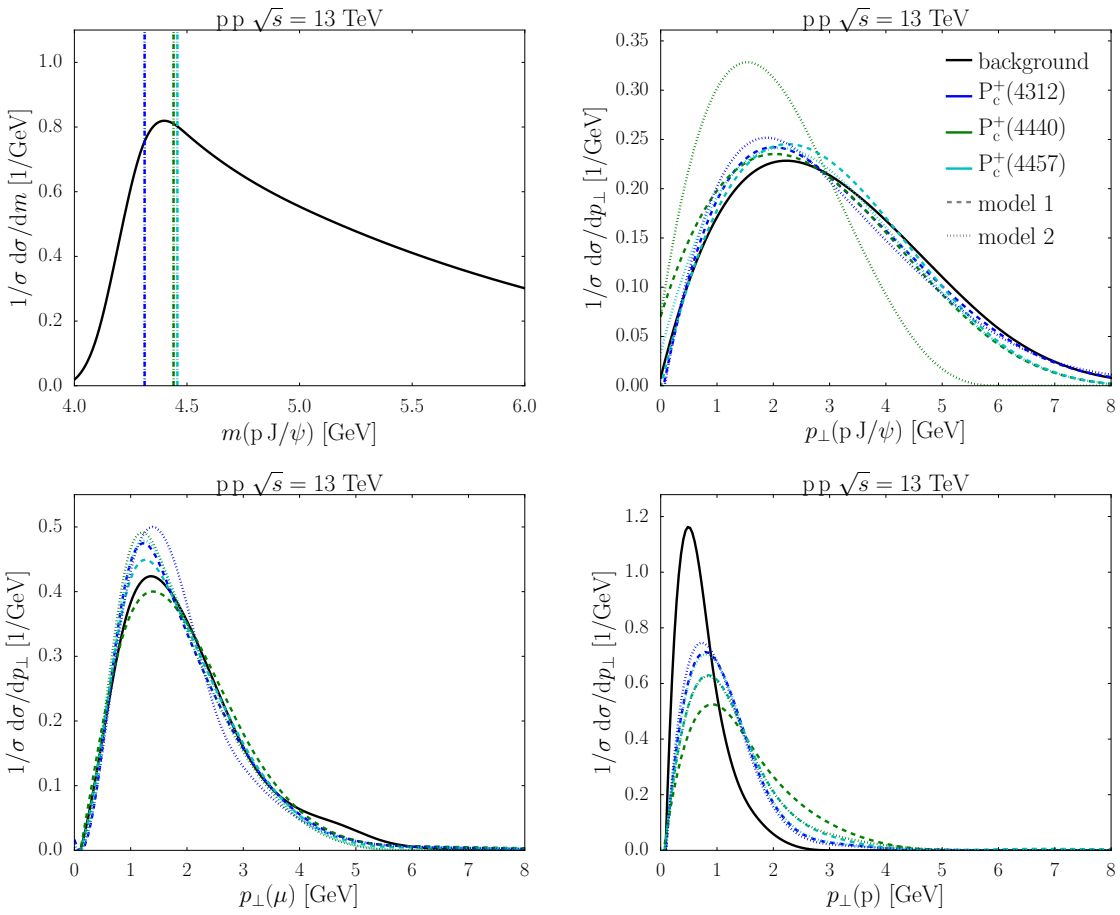

Figure 6: Normalised cross-sections for $\mathrm{P_c^+} \to \mathrm{p\,J/\psi}$ decays and (solid black) combinatorial background, differential in (top left) final-state mass, (top right) final-state $p_\perp$, (bottom left) muon $p_\perp$, and (bottom right) proton $p_\perp$.

Table 4: Expected number of reconstructed prompt background and signal $\mathrm{P_c^+}$ candidates by the LHCb detector during Run 3.

	bkg	$\mathrm{P_c^+(4312)}$	$\mathrm{P_c^+(4440)}$	$\mathrm{P_c^+(4457)}$
model 1	2×10^8	2×10^2	2×10^2	1×10^2
model 2		1×10^4	5×10^3	8×10^3

is sufficient. From Table 4 it is clear that prompt P_c^+ production from hadronic rescattering, given the models considered here, will not be observable by LHCb. However, even limits on prompt P_c^+ production will still provide a valuable tool in understanding the nature of the observed pentaquark states.

4 Conclusion

The hadronic rescattering framework in PYTHIA has been modified to allow for the production of arbitrary hadronic resonances, with an emphasis placed on the production of exotic hadrons that may be molecular states. The relevant code will be published in an upcoming PYTHIA release. The production cross sections for the tetraquark candidate $\chi_{c1}(3872)$, and the pentaquark candidates $P_c^+(4312)$, $P_c^+(4440)$, and $P_c^+(4457)$, have been calculated for $\sqrt{s} = 13$ TeV p p collisions at the LHC. Using this implementation of PYTHIA, hadronic rescattering predictions could also be made for the additional exotic states discovered at the LHC. The hadronic rescattering cross section for $\chi_{c1}(3872)$ production at $\sqrt{s} = 7$ TeV in p p collisions is compared to the inclusive $\chi_{c1}(3872)$ cross-section measurement by LHCb and found to contribute at a 1% level. Finally, the expected number of prompt P_c^+ candidates from hadronic rescattering observed by LHCb during Run 3, using the exclusive final state of $p J/\psi[\to \mu^+ \mu^-]$, is estimated and found to be significantly smaller than the estimated prompt background. However, cross-section measurements of the P_c^+ candidates, separated into prompt and displaced contributions, can still differentiate between predicted molecular models of these pentaquarks.

Acknowledgements

The authors would like to thank Stephen Mrenna for initial discussions about modelling pentaquark formation and Torbjörn Sjöstrand for further general discussion. PI is supported by the U.S. National Science Foundation grant OAC-2103889. MU is supported in part by the Swedish Research Council, contract number 2016-05996, and in part by the MCnetITN3 H2020 Marie Curie Innovative Training Network, grant agreement 722104.

References

[1] M. Gell-Mann, "A Schematic Model of Baryons and Mesons," *Phys. Lett.* **8** (1964) 214–215.

[2] G. Zweig, *An SU(3) model for strong interaction symmetry and its breaking. Version 2.* 2, 1964.

[3] R. L. Jaffe, "Multi-Quark Hadrons. 1. The Phenomenology of (2 Quark 2 anti-Quark) Mesons," *Phys. Rev. D* **15** (1977) 267.

[4] D. Strottman, "Multi - Quark Baryons and the MIT Bag Model," *Phys. Rev. D* **20** (1979) 748–767.

[5] H. J. Lipkin, "New Possibilities for Exotic Hadrons: Anticharmed Strange Baryons," *Phys. Lett. B* **195** (1987) 484–488.

[6] K. H. Hicks, "On the conundrum of the pentaquark," *Eur. Phys. J. H* **37** (2012) 1–31.

[7] **Belle** Collaboration, S. K. Choi *et. al.*, "Observation of a resonance-like structure in the $pi^{\pm}\psi'$ mass distribution in exclusive $B \to K\pi^{\pm}\psi'$ decays," *Phys. Rev. Lett.* **100** (2008) 142001, 0708.1790.

[8] **Belle** Collaboration, S. K. Choi *et. al.*, "Observation of a narrow charmonium - like state in exclusive B+- —> K+- pi+ pi- J / psi decays," *Phys. Rev. Lett.* **91** (2003) 262001, hep-ex/0309032.

[9] **LHCb** Collaboration, R. Aaij *et. al.*, "Observation of $J/\psi p$ Resonances Consistent with Pentaquark States in $\Lambda_b^0 \to J/\psi K^- p$ Decays," *Phys. Rev. Lett.* **115** (2015) 072001, 1507.03414.

[10] **LHCb** Collaboration, R. Aaij *et. al.*, "Observation of a narrow pentaquark state, $P_c(4312)^+$, and of two-peak structure of the $P_c(4450)^+$," *Phys. Rev. Lett.* **122** (2019), no. 22 222001, 1904.03947.

[11] **BaBar** Collaboration, B. Aubert *et. al.*, "Study of the $B \to J/\psi K^- \pi^+ \pi^-$ decay and measurement of the $B \to X(3872) K^-$ branching fraction," *Phys. Rev. D* **71** (2005) 071103, hep-ex/0406022.

[12] **LHCb** Collaboration, R. Aaij *et. al.*, "Determination of the X(3872) meson quantum numbers," *Phys. Rev. Lett.* **110** (2013) 222001, 1302.6269.

[13] **LHCb** Collaboration, R. Aaij *et. al.*, "Quantum numbers of the $X(3872)$ state and orbital angular momentum in its $\rho^0 J\psi$ decay," *Phys. Rev. D* **92** (2015), no. 1 011102, 1504.06339.

[14] N. A. Tornqvist, "Isospin breaking of the narrow charmonium state of Belle at 3872-MeV as a deuson," *Phys. Lett. B* **590** (2004) 209–215, hep-ph/0402237.

[15] L. Maiani, F. Piccinini, A. D. Polosa, and V. Riquer, "Diquark-antidiquarks with hidden or open charm and the nature of X(3872)," *Phys. Rev. D* **71** (2005) 014028, hep-ph/0412098.

[16] **BaBar** Collaboration, B. Aubert *et. al.*, "Search for a charged partner of the X(3872) in the B meson decay $B \to X^- K$, $X^- \to J/\psi \pi^- \pi^0$," *Phys. Rev. D* **71** (2005) 031501, hep-ex/0412051.

[17] L. Maiani, A. D. Polosa, and V. Riquer, "A Theory of X and Z Multiquark Resonances," *Phys. Lett. B* **778** (2018) 247–251, 1712.05296.

[18] C. Bignamini, B. Grinstein, F. Piccinini, A. D. Polosa, and C. Sabelli, "Is the X(3872) Production Cross Section at Tevatron Compatible with a Hadron Molecule Interpretation?," *Phys. Rev. Lett.* **103** (2009) 162001, 0906.0882.

[19] P. Artoisenet and E. Braaten, "Production of the X(3872) at the Tevatron and the LHC," *Phys. Rev. D* **81** (2010) 114018, 0911.2016.

[20] F.-K. Guo, U.-G. Meißner, W. Wang, and Z. Yang, "Production of charm-strange hadronic molecules at the LHC," *JHEP* **05** (2014) 138, 1403.4032.

[21] M. Albaladejo, F.-K. Guo, C. Hanhart, U.-G. Meißner, J. Nieves, A. Nogga, and Z. Yang, "Note on X(3872) production at hadron colliders and its molecular structure," *Chin. Phys. C* **41** (2017), no. 12 121001, 1709.09101.

[22] R. Chen, X. Liu, X.-Q. Li, and S.-L. Zhu, "Identifying exotic hidden-charm pentaquarks," *Phys. Rev. Lett.* **115** (2015), no. 13 132002, 1507.03704.

[23] H.-X. Chen, W. Chen, X. Liu, T. G. Steele, and S.-L. Zhu, "Towards exotic hidden-charm pentaquarks in QCD," *Phys. Rev. Lett.* **115** (2015), no. 17 172001, 1507.03717.

[24] J. He, "$\bar{D}\Sigma_c^*$ and $\bar{D}^*\Sigma_c$ interactions and the LHCb hidden-charmed pentaquarks," *Phys. Lett. B* **753** (2016) 547–551, 1507.05200.

[25] H. Huang, C. Deng, J. Ping, and F. Wang, "Possible pentaquarks with heavy quarks," *Eur. Phys. J. C* **76** (2016), no. 11 624, 1510.04648.

[26] L. Roca and E. Oset, "On the hidden charm pentaquarks in $\Lambda_b \to J/\psi K^- p$ decay," *Eur. Phys. J. C* **76** (2016), no. 11 591, 1602.06791.

[27] Q.-F. Lü and Y.-B. Dong, "Strong decay mode $J/\psi p$ of hidden charm pentaquark states $P_c^+(4380)$ and $P_c^+(4450)$ in $\Sigma_c \bar{D}^*$ molecular scenario," *Phys. Rev. D* **93** (2016), no. 7 074020, 1603.00559.

[28] Y. Shimizu, D. Suenaga, and M. Harada, "Coupled channel analysis of molecule picture of $P_c(4380)$," *Phys. Rev. D* **93** (2016), no. 11 114003, 1603.02376.

[29] C.-W. Shen, F.-K. Guo, J.-J. Xie, and B.-S. Zou, "Disentangling the hadronic molecule nature of the $P_c(4380)$ pentaquark-like structure," *Nucl. Phys. A* **954** (2016) 393–405, 1603.04672.

[30] Y. Yamaguchi, A. Giachino, A. Hosaka, E. Santopinto, S. Takeuchi, and M. Takizawa, "Hidden-charm and bottom meson-baryon molecules coupled with five-quark states," *Phys. Rev. D* **96** (2017), no. 11 114031, 1709.00819.

[31] S. Dubynskiy and M. B. Voloshin, "Hadro-Charmonium," *Phys. Lett. B* **666** (2008) 344–346, 0803.2224.

[32] M. Karliner and B. R. Webber, "Coalescence model for Theta(c) pentaquark formation," *JHEP* **12** (2004) 045, hep-ph/0409121.

[33] P. Ling, X.-H. Dai, M.-L. Du, and Q. Wang, "Prompt production of the hidden charm pentaquarks in the LHC," 2104.11133.

[34] T. Sjöstrand, S. Ask, J. R. Christiansen, R. Corke, N. Desai, P. Ilten, S. Mrenna, S. Prestel, C. O. Rasmussen, and P. Z. Skands, "An introduction to PYTHIA 8.2," *Comput. Phys. Commun.* **191** (2015) 159–177, 1410.3012.

[35] T. Sjöstrand and M. Utheim, "A Framework for Hadronic Rescattering in pp Collisions," *Eur. Phys. J. C* **80** (2020), no. 10 907, 2005.05658.

[36] C. Bierlich, T. Sjöstrand, and M. Utheim, "Hadronic rescattering in pA and AA collisions," *Eur. Phys. J. A* **57** (2021), no. 7 227, 2103.09665.

[37] **Particle Data Group** Collaboration, P. A. Zyla *et. al.*, "Review of Particle Physics," *PTEP* **2020** (2020), no. 8 083C01.

[38] **LHCb** Collaboration, R. Aaij *et. al.*, "Study of the lineshape of the $\chi_{c1}(3872)$ state," *Phys. Rev. D* **102** (2020), no. 9 092005, 2005.13419.

[39] **LHCb** Collaboration, R. Aaij *et. al.*, "Study of the $\psi_2(3823)$ and $\chi_{c1}(3872)$ states in $B^+ \to (J\psi\pi^+\pi^-)\, K^+$ decays," *JHEP* **08** (2020) 123, 2005.13422.

[40] Y.-H. Lin and B.-S. Zou, "Strong decays of the latest LHCb pentaquark candidates in hadronic molecule pictures," *Phys. Rev. D* **100** (2019), no. 5 056005, 1908.05309.

[41] E. M. Levin and L. L. Frankfurt, "The Quark hypothesis and relations between cross-sections at high-energies," *JETP Lett.* **2** (1965) 65–70.

[42] H. J. Lipkin, "Quarks for pedestrians," *Phys. Rept.* **8** (1973) 173–268.

[43] **Particle Data Group** Collaboration, M. Tanabashi *et. al.*, "Review of Particle Physics," *Phys. Rev. D* **98** (2018), no. 3 030001.

[44] S. A. Bass *et. al.*, "Microscopic models for ultrarelativistic heavy ion collisions," *Prog. Part. Nucl. Phys.* **41** (1998) 255–369, nucl-th/9803035.

[45] **LHCb** Collaboration, R. Aaij *et. al.*, "Study of the production of Λ_b^0 and $\overline{B}^0$ hadrons in pp collisions and first measurement of the $\Lambda_b^0 \to J/\psi p K^-$ branching fraction," *Chin. Phys. C* **40** (2016), no. 1 011001, 1509.00292.

[46] P. Z. Skands, "Tuning Monte Carlo Generators: The Perugia Tunes," *Phys. Rev. D* **82** (2010) 074018, 1005.3457.

[47] **ATLAS** Collaboration, M. Aaboud *et. al.*, "Measurement of the Inelastic Proton-Proton Cross Section at $\sqrt{s} = 13$ TeV with the ATLAS Detector at the LHC," *Phys. Rev. Lett.* **117** (2016), no. 18 182002, 1606.02625.

[48] **CMS** Collaboration, A. M. Sirunyan *et. al.*, "Measurement of the inelastic proton-proton cross section at $\sqrt{s} = 13$ TeV," *JHEP* **07** (2018) 161, 1802.02613.

[49] **LHCb** Collaboration, R. Aaij *et. al.*, "Measurement of the inelastic pp cross-section at a centre-of-mass energy of 13 TeV," *JHEP* **06** (2018) 100, 1803.10974.

[50] **TOTEM** Collaboration, G. Antchev *et. al.*, "First measurement of elastic, inelastic and total cross-section at $\sqrt{s} = 13$ TeV by TOTEM and overview of cross-section data at LHC energies," *Eur. Phys. J. C* **79** (2019), no. 2 103, 1712.06153.

[51] **ATLAS** Collaboration, M. Aaboud *et. al.*, "Measurement of charged-particle distributions sensitive to the underlying event in $\sqrt{s} = 13$ TeV proton-proton collisions with the ATLAS detector at the LHC," *JHEP* **03** (2017) 157, 1701.05390.

[52] **CMS** Collaboration, V. Khachatryan *et. al.*, "Pseudorapidity distribution of charged hadrons in proton-proton collisions at $\sqrt{s} = 13$ TeV," *Phys. Lett. B* **751** (2015) 143–163, 1507.05915.

[53] **LHCb** Collaboration, R. Aaij *et. al.*, "Measurement of charged particle multiplicities in pp collisions at $\sqrt{s} = 7$TeV in the forward region," *Eur. Phys. J. C* **72** (2012) 1947, 1112.4592.

[54] **LHCb** Collaboration, R. Aaij *et. al.*, "Measurement of the forward energy flow in pp collisions at $\sqrt{s} = 7$ TeV," *Eur. Phys. J. C* **73** (2013) 2421, 1212.4755.

[55] **LHCb** Collaboration, R. Aaij *et. al.*, "Measurement of prompt hadron production ratios in pp collisions at $\sqrt{s} = 0.9$ and 7 TeV," *Eur. Phys. J. C* **72** (2012) 2168, 1206.5160.

[56] **LHCb** Collaboration, R. Aaij *et. al.*, "Measurement of V^0 production ratios in pp collisions at $\sqrt{s} = 0.9$ and 7 TeV," *JHEP* **08** (2011) 034, 1107.0882.

[57] **LHCb** Collaboration, R. Aaij *et. al.*, "Measurements of prompt charm production cross-sections in pp collisions at $\sqrt{s} = 13$ TeV," *JHEP* **03** (2016) 159, 1510.01707. [Erratum: JHEP 09, 013 (2016), Erratum: JHEP 05, 074 (2017)].

[58] **LHCb** Collaboration, R. Aaij *et. al.*, "Observation of $X(3872)$ production in pp collisions at $\sqrt{s} = 7$ TeV," *Eur. Phys. J. C* **72** (2012) 1972, 1112.5310.

[59] **LHCb** Collaboration, I. Bediaga *et. al.*, "Framework TDR for the LHCb Upgrade: Technical Design Report,".

[60] **LHCb** Collaboration, I. Bediaga, "LHCb VELO Upgrade Technical Design Report,".

[61] **LHCb** Collaboration, "LHCb PID Upgrade Technical Design Report,".

[62] **LHCb** Collaboration, "LHCb Tracker Upgrade Technical Design Report,".

[63] "LHCb Trigger and Online Upgrade Technical Design Report,".

[64] **LHCb** Collaboration, R. Aaij *et. al.*, "Physics case for an LHCb Upgrade II - Opportunities in flavour physics, and beyond, in the HL-LHC era," 1808.08865.

[65] **LHCb** Collaboration, R. Aaij *et. al.*, "LHCb Detector Performance," *Int. J. Mod. Phys. A* **30** (2015), no. 07 1530022, 1412.6352.